Available online at www.sciencedirect.com
SCIENCE DIRECT®
Tetrahedron: Asymmetry
Tetrahedron: *Asymmetry* 16 (2005) 519–527

The conformational behaviour of α,β-trehalose-like disaccharides and their *C*-glycosyl, imino-*C*-glycosyl and carbagalactose analogues depends on the chemical nature of the modification: an NMR investigation

Víctor García-Aparicio,[a] María del Carmen Fernández-Alonso,[a] Jesús Angulo,[c] Juan Luis Asensio,[b] Fco. Javier Cañada,[a] Jesús Jiménez-Barbero,[a,*] David R. Mootoo[d,*] and Xuhong Cheng[d]

[a]*Departamento de Estructura y Función de Proteínas, Centro de Investigaciones Biológicas, CSIC, Ramiro de Maeztu 9, 28040 Madrid, Spain*
[b]*Instituto de Química Orgánica, CSIC, Amércio Vespucio s/n 41092 Madrid, Spain*
[c]*Instituto de Investigaciones Químicas, CSIC, Juan de la Cierva 3, 28006 Seville, Spain*
[d]*Hunter College of the City University of New York, 695 Park Ave, New York, NY 10021, USA*

Received 15 November 2004; accepted 29 November 2004
Available online 22 December 2004

Abstract—The conformational behaviour of β-*O*-Gal-(1→1)-α-Man **4** and the *C*-glycoside, carbaglycoside and aza-*C*-glycoside mimics **1**–**3** has been studied using *J*/NOE NMR data, molecular mechanics and molecular dynamics. It is shown that the population distributions around the glycosidic linkages of the different analogues depend on the chemical nature of the acetal or pseudo-acetal residue.

1. Introduction

Carbohydrate–protein interactions are involved in a wide variety of biological cell–cell recognition events including fertilization, virus infections or even tumor growth.[1] Sugar mimics that are able to bind viral and microbial surface lectins thereby providing potential protection against infection, have recently been the subject of intensive research.[2] *C*-Glycosyl and carbaglycosyl in which the *endo* or *exo* glycosidic oxygen in the natural *O*-glycosides is, respectively, replaced with a methylene group have been developed primarily because of their chemical and enzymatic stability.[3] For these compounds to be biologically useful as potential drug candidates, it is important that they exhibit similar three-dimensional structures as the parent *O*-glycosides, so that the recognition process is not compromised.[4] However, the substitution of the acetal oxygen atoms by methylene groups results in changes in the size and electronic properties of the associated atoms and in bond distances and consequently the flexibility and population distributions around the inter-residue linkages are expected to be affected.[5,6]

Following our earlier studies in this area, we report here on the conformational behaviour (in water) of the trehalose-type analogues **1**–**3** (Fig. 1), in comparison with the *O*-glycosyl parent compound, **4**.[7] Our initial interest in this set of analogues stems from the hypothesis that **4** is a mimic of sLeX, which is five times as active as sLeX in binding to E-Selectin.[8] Moreover, comparison of the conformational behaviour of compounds **1**–**4** provide a means to evaluate the relative role of steric and stereoelectronic effects in determining the conformational preferences of saccharides and analogues. Our results on the nonsubstituted analogues of **1** and **4** (**1b** and **4b**, lacking the CH_2COOH chain) have been previously reported.[9]

The protocol we have used is based on a combination of NMR spectroscopy and molecular mechanics and

* Corresponding authors. E-mail: jjbarbero@cib.csic.es

0957-4166/$ - see front matter © 2004 Published by Elsevier Ltd.
doi:10.1016/j.tetasy.2004.11.072

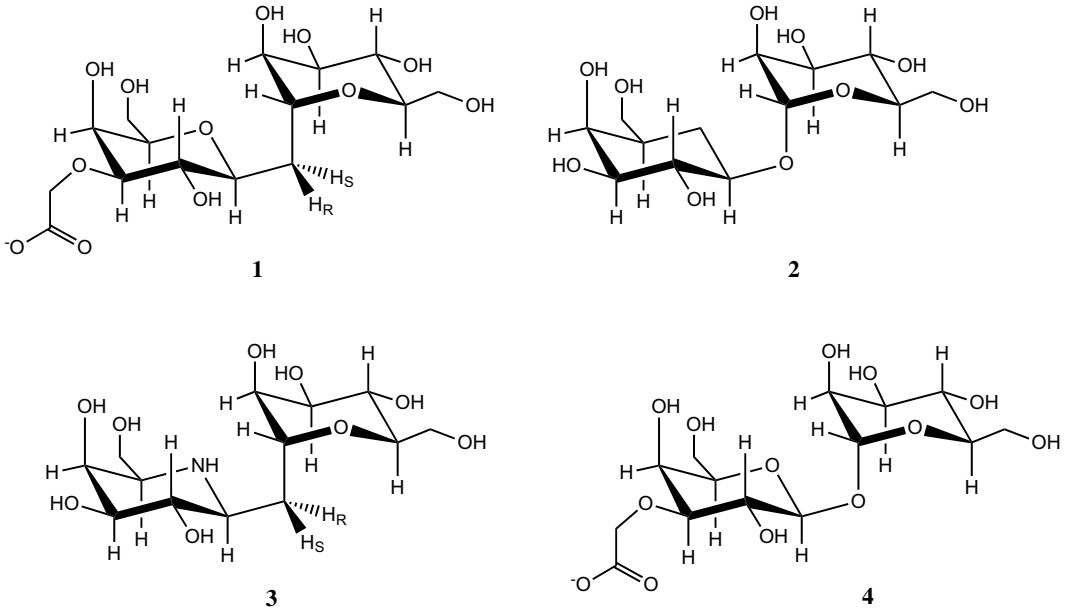

Figure 1. Trehalose-type analogues **1**–**3** and their parent O-linked disaccharides **4**.

dynamics calculations. This approach has been demonstrated to be particularly useful for the determination of the conformational properties of other glycomimetics.[10]

2. Results and discussion

2.1. Molecular mechanics and dynamics calculations

The potential energy surfaces of all compounds were calculated using the MM3*[11] force field, as previously described.[9,12,13] These maps are useful to delimit the low-energy regions that are accessible to rotation around the glycosidic torsion angles Φ_{Gal} and Φ_{Man} (see Table 1). The substitution at position 3 of the galactose moiety in **1** and **4** did not modify the shape of the potential energy maps, which are basically identical to those described previously for the unsubstituted analogues **1b** and **4b**.[9] The potential energy maps for **2** and **3** are given in Figure 2. As shown in Table 1, the MM3* force field predict that compounds **1**–**4** have distinct conformational behaviour, depending on their chemical nature.

Table 1. Comparison between the inter-residue proton–proton distances deduced by MM3* calculations for the **A**–**E** conformers of **1**–**4** (approximated Φ_{Gal} and Φ_{Man} angles between brackets) and the observed NOEs for **1**–**4**

Conformer Φ/Ψ	**NOE** exp (**1**)	NOE exp (**2**)	NOE exp (**3**)	NOE exp (**4**)	**A** 60/60	**B** 50/−50	**C** −60/−60	**D** −170/60	**E** 160/−60
ΔE (**1**)	—	—	—	—	5.9	0.0	9.3	9.6	7.7
ΔE (**2**)	—	—	—	—	12	0.2	0.0	34.2	12.8
ΔE (**3**)	—	—	—	—	6.3	0.0	5.9	7.9	5.5
ΔE (**4**)	—	—	—	—	3.4	0.0	3.7	6.5	3.4
1G-1M	MS	S	S	S	3.1	**2.5**	3.1	3.7	3.5
1G-5M	MW	VW	W	VW	4.5	4.2	**2.7**	4.5	4.1
1G-2M	MS	W	W	VW	**2.0**	4.3	4.6	3.4	4.6
1G-3M	VW	VW	VW	N.D.	**3.1**	5.1	4.2	3.8	4.9
R-2G	MS	—	M	—	**2.5**	**2.5**	3.7	2.9	2.9
R-2M	W	—	W	—	3.8	3.1	2.9	3.8	3.2
R-5M	S	—	S	—	3.0	2.2	2.3	3.0	2.0
S-5M	S	—	M	—	**2.2**	3.7	3.8	**2.1**	3.7
R-3M	S	—	S	—	3.9	2.4	2.2	2.9	2.4
S-3M	MS	—	M	—	**2.2**	3.1	3.4	**2.3**	3.1
S-2M	S	—	S	—	3.0	2.4	2.6	3.1	2.4
S-2G	M	—	M	—	3.1	3.0	**2.4**	3.8	3.8
1M-2G	W	N.D.	VW	N.D.	4.2	4.7	2.9	**2.1**	**2.6**
5M-2G	VW	VW	VW	VW	5.0	4.0	5.1	5.1	**2.8**
2G-2M	VW	N.D.	VW	N.D.	4.7	5.3	4.4	**2.3**	4.6
7′eqG-1M	—	MS	—	—	2.3	2.7	4.2	—	2.5
7′eqG-5M	—	MW	—	—	4.7	3.5	**2.3**	—	4.9
7′axG-5M	—	M	—	—	4.3	**2.6**	3.4	—	4.1
7′axG-1M	—	VW	—	—	3.4	3.8	4.7	—	**1.9**

Relative steric energies for **1**–**4** (ΔE, kJ/mol) are also given. Exclusive NOEs[16] and NOEs, which may correspond to two conformers are shown in bold. Conformer **D** of **2** is no longer local minimum.

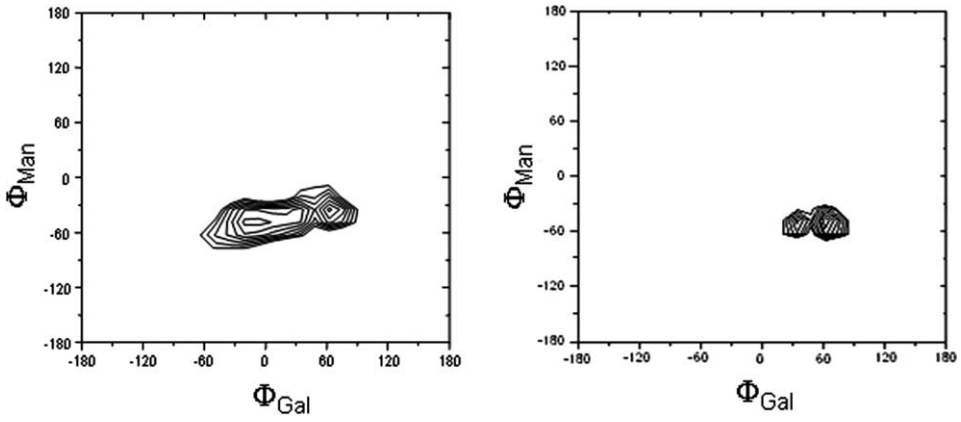

Figure 2. Steric energy maps calculated by MM3* with $\varepsilon = 80$. Left for **2** and right **3**. Contours are given every 2 kJ mol^{-1}.

Several low-energy conformers with appreciable populations (Fig. 3) are calculated for compounds **1** and **3**, in marked contrast with the *O*-glycosyl compound, **4**, for which a very major conformation is predicted. As was earlier shown for **4b** in water, a double *exo*-anomeric conformation around both Φ_{Gal} and Φ_{Man} torsion angles is expected, with a population above 95%.[14] The different conformers have been dubbed, according to the orientation around the pseudoglycosidic linkages, that is, *exo*, non-*exo* or *anti*, by considering their accordance or not with the *exo*-anomeric geometry (when Φ, defined as H1–C1–X–C1′, shows a +60° value adopts an *exo*-orientation in β-glycosides, while Φ is ca. −60° in α-glycosides, also corresponds to an *exo*-anomeric conformation), or their disposition in an *anti*-type arrangement (Φ ca. 180°) (**A**) *exo*-Φ_{Gal}/non-*exo*-Φ_{Man}, (**B**) *exo*-Φ_{Gal}/*exo*-Φ_{Man}, (**C**) non-*exo*-Φ_{Gal}/*exo*-Φ_{Man}, (**D**) *anti*-Φ_{Gal}/non-*exo*-Φ_{Man}, (**E**) *anti*-Φ_{Gal}/*exo*-Φ_{Man}. According to the MM3* calculations, conformer **B**, with the double *exo*-anomeric orientation is the major one (90%) for compound **1**, followed by the *exo*-Φ_{Gal}/non-*exo*-Φ_{Man} conformer (7%) and *anti*-Φ_{Gal}/non-*exo*-Φ_{Man} conformer (3%). Compound **3** also shows the same energy minima, although with slightly different relative steric energies and populations. In both cases, the *anti*-Φ_{Gal} geometry is also relevant, according to the MM3* calculations.[15] In contrast, *anti*-conformers are more destabilized for **2**, and there is a mixture of two conformers *exo*-Φ_{Gal}/*exo*-Φ_{Man} and non-*exo*-Φ_{Gal}/*exo*-Φ_{Man}, with slightly predominance of last one. Finally, and as already described for **4b**, a very major *exo*-Φ_{Gal}/*exo*-Φ_{Man} conformer (>99%) with overlapping *exo*-anomeric effects is predicted for the *O*-glycosyl compound, **4**. The relative energies and the key geometrical features of these conformers are shown in Table 1.

It can be observed that there are a number of key proton–proton short distances (<3 Å) that are exclusive of the different conformers. That is, its observation in the NOE spectra (see below) should indicate the presence of the corresponding conformer in the conformational equilibrium. In short, for **1** and **3**, they are H1Gal–H1Man (conformer **B**, double *exo*), H1Gal–H2Man (conformer **A**, non-*exo* at the Man linkage), H2Gal–H2Man (conformers **D**, with a non-*exo* arrangement at the Man linkage and *anti*-orientation at the Gal linkage), H2Gal–HproS (conformer C, with the non-*exo* geometry at the Gal linkage), and H2Gal–H1Man (conformers **D** and/or **E**, *anti* orientation at the Gal linkage). In the case of compound **2** (see Table 1), in addition, the H7axGal–H5Man is exclusive of **B**, the H7axGal–H1Man is exclusive of **E**, and the H7eqGal–H5Man is exclusive of **C**. As a further step, the conformational stability of the different conformers of **1**–**4** was checked by using MD simulations[17] also with the MM3* (data not shown) force field. Some of the computed Φ/Ψ distributions are displayed in Figure 4 for all compounds, while the average distances of several key H/H distances that may be related to observed NOEs (see below) are shown in Table 2.

The numeric values of these distances in comparison to those expected from the experimental NOE data (see below), calculated according to a full relaxation matrix approach, are gathered in Table 2.

Again, different behaviours are observed among the different compounds, according to the simulations. The simulations are markedly similar to the probability distributions obtained by the systematic molecular mechanics approach. Again, for compounds **1**–**3**, the MM3*-based MD simulations (Fig. 4) predict the existence of conformational equilibria between at least three conformers. In particular, the (**A**) *exo*-Φ_{Gal}/non-*exo*-Φ_{Man} (only for compound **1**) and (**B**) *exo*-Φ_{Gal}/*exo*-Φ_{Man} (major for both compounds) geometries dominate the distributions, with additional contributions of the *anti*-Φ_{Gal}/*exo*-Φ_{Man} (only for compound **1**) geometry. Minor sampling of the other two conformers is also observed. For compound **2** there is an equilibrium between (**A**) *exo*-Φ_{Gal}/non-*exo*-Φ_{Man} and (**B**) *exo*-Φ_{Gal}/*exo*-Φ_{Man}, in contrast with compound, **4**, for which (**B**) *exo*-Φ_{Gal}/*exo*-Φ_{Man} is predicted the major conformer in solution.

2.2. NMR spectroscopy

The predictions of the force field calculations were checked by using NMR to get the final conformational distribution for **1**–**4**. The chemical shifts in D_2O of **1**–**4** are listed in Table 3. The assignment of the resonances

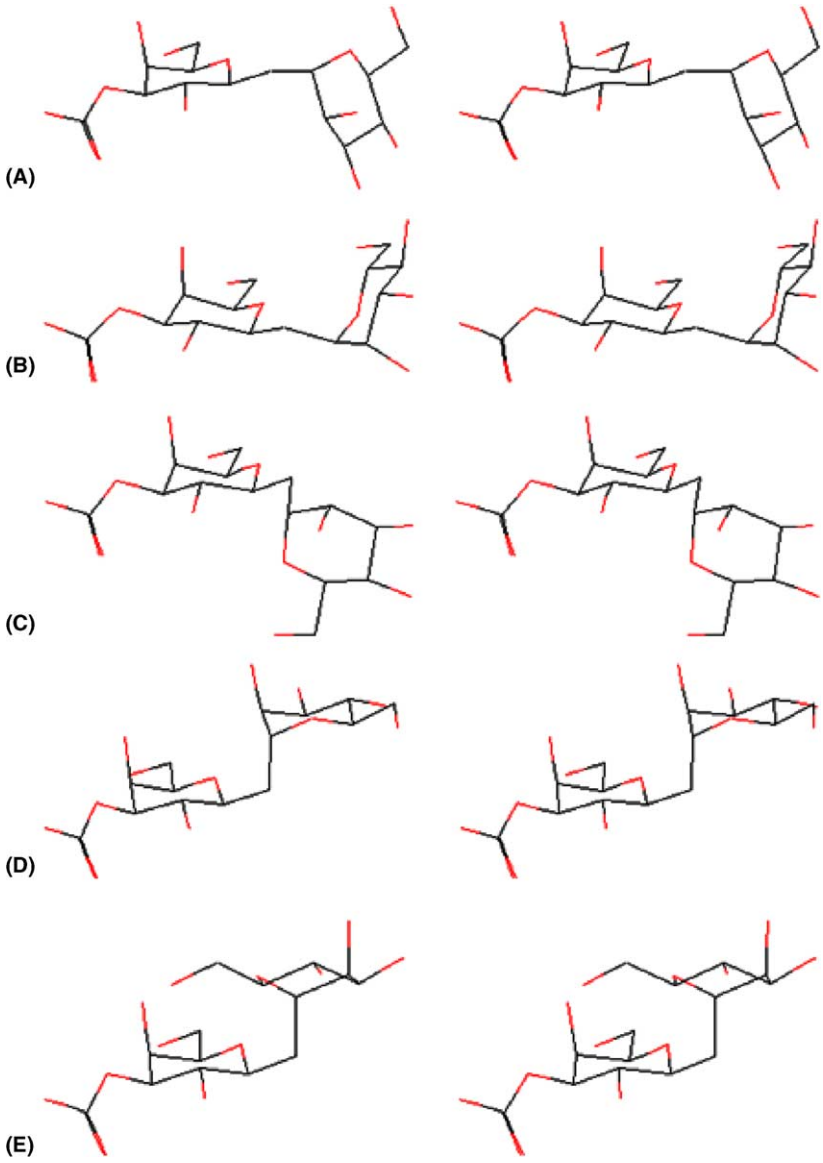

Figure 3. Stereoviews of the global and local minima of **1** according to MM3* calculations. (A) Conformer **A**; (B) conformer **B**; (C) conformer **B**; (D) conformer **D**; (E) conformer **E**. See Table 1 for the Φ and Ψ torsions of the different conformers. These five local minimum are the same for compounds **2**–**4**.

was made through a combination of COSY, TOCSY, 1D and 2D-NOESY/ROESY, and HSQC experiments (Fig. 5).

The J values for the ring protons indicate that all the pyranose chairs adopt the usual $^4C_1$ chair, independently of the size of the molecule and of the nature of the *C*- or *O*-glycosidic linkage. Although this is usually the case, in some cases alternative chair conformations have been described for other *C*-glycosyl compounds.[18] The intermediate observed values for the C5–C6 lateral chains are in agreement with equilibria between the tg:gt conformers for the Gal/pseudoGal rings and the gg:gt conformers for the Man moieties.[19]

In a second step, NOESY and ROESY experiments were carried out to deduce the relevant conformational information. The intensities of the observed NOES (Fig. 4) compared to those estimated by the MM3* molecular mechanics and dynamics calculations, calculated according to a full relaxation matrix approach are also gathered in Tables 1 and 2. The analysis of the conformational behaviour of **1** and **3** was also facilitated by the analysis of the measured interglycosidic J values between the prochiral methylene protons and the H-1Gal and H-1Man protons at the glycosidic positions. In particular, for **1** and **3**, as shown in Table 4, the observed scalar couplings indicate the existence of conformational equilibria with respect to both glycosidic torsions.

For **1**, by considering the basic conformers around both torsions and their corresponding expected coupling constants (Table 3), a 70:30 equilibrium among the *exo*/*anti* staggered conformers around Φ_{Gal} and an almost equivalent distribution between the two possible *exo*:non-*exo*

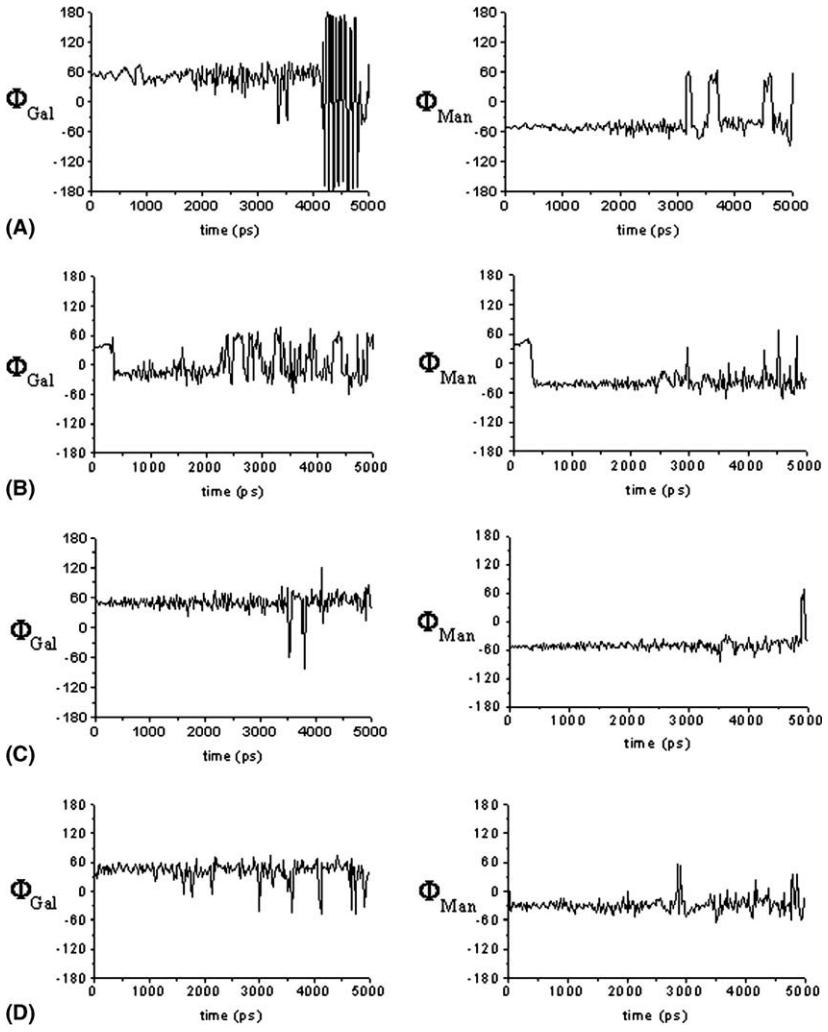

Figure 4. Frequency of sampling of Φ/Ψ torsion angles from the MD simulations (MM3*) for **1**–**4**. From top to bottom (A) compound **1**; (B) compound **2**; (C) compound **3**; (D) compound **4**.

staggered conformers around Φ_{Man} matches the observed couplings in a satisfactory manner. Therefore, just with this qualitative coupling constants analysis and considering the geometries from molecular mechanics, it may be extrapolated that the double *exo*-anomeric conformer is not the dominant one in solution, and that the *exo*-Gal/non-*exo*-Man one also contributes significantly. Thus, the population of the double *exo*-anomeric conformer **B** of **1** seems to be largely overestimated by the MM3* simulations (from 90% to less than 50%). In contrast, the actual conformation of **A** in solution should be higher than that predicted by MM3* (7%). A different behaviour is observed for **3**. In this case, the large values of the couplings clearly indicate that the double *exo*-conformer dominates the conformational equilibrium. Indeed, a distribution of with more than 80% of *exo*-anomeric conformers around both Φ_{Gal} and Φ_{Man} matches the observed couplings in a very satisfactorily way. Therefore, the presence of the nitrogen atom at the *endo*-glycosidic position of the galactose moiety produces a significant shifting of population towards the double *exo*-anomeric conformer at expense of the other non-*exo* and *anti* geometries. Now, the population of conformer **B** should be around 80%.

These semiquantitative observations were further confirmed by using NOE measurements (Fig. 5). For **1** and **3**, the simultaneous presence of the exclusive H-1Gal/H-1Man, H-2Gal/H-1Man, H-2Gal/H-2Man and H-1Gal/H-2Man NOEs cannot be explained by considering a single or even an equilibrium between two conformers. The additional presence of strong NOE for **1** and **3** (Table 1) between the H2Gal–HproR protons pair indicate that the *exo*-Φ conformer at the Gal linkage should be indeed present in a high percentage in solution. Nevertheless, the presence of a medium intensity H2Gal–HproS cross peak suggests that this is not the only conformer present in equilibrium, and that the *non-exo* geometry also participates in the equilibrium. Regarding the Φ-Man linkage, a certain proportion of the *non-exo* needs also to be accounted for to justify the H3Man–HproS and H5Man–HproS contacts. For **2**, the simultaneous presence of H1Gal–H1Man, H1Gal–H2Man, H7eqGal–H1Man, H7eqGal–H5Man and H7axGal–H5Man NOEs (Fig. 5) permitted again to verify the existence of a conformational equilibrium in which at least conformers **A**, **B** and **C** take place. The cross peak H7eq–H5Man is more intense than H7ax–H5Man that implies conformer **C** is more

Table 2. Expected distances estimated from the molecular mechanics (MM) and molecular dynamics simulations (MD)

Proton pair	Average distances from MM and MD (Å)				NOEs estimated from MM/MD calculations according to a full matrix relaxation approach (%)				Observed NOEs (%)			
	1	**2**	**3**	**4**	**1**	**2**	**3**	**4**	**1**	**2**	**3**	**4**
1G-1M	2.4	2.4	2.4	2.4	6	13	6	11.6	6.9	12	6.8	12.3
1G-5M	3.7	3.7	3.7	4.1	—	—	—	0.5	—	—	—	1
1G-2M	3.6	3.6	3.6	3.9	1.5	1.5	1.5	—	2.2	1.4	1.8	—
1G-3M	4.3	4.3	4.3	4.7	—	—	—	—	—	—	—	—
R-2G	2.7	—	2.7	—	3.6	—	1	—	4.7	—	1.5	—
R-2M	3.1	—	2.4	—	0	—	9	—	0	—	8.5	—
R-5M	2.2	—	3.0	—	14	—	2	—	12.4	—		—
S-5M	3.0	—	2.2	—	2.1	—	12	—	2.3	—	11.2	—
R-3M	2.6	—	2.6	—	4.2	—	0	—	3.5	—	0	—
S-3M	2.9	—	2.4	—	2.1	—	4	—	1.8	—	3.4	—
S-2M	2.4	—	3.2	—	5.9	—	1	—	5.2	—	1.8	—
S-2G	2.8	—	2.9	—	2.3	—	4	—	1.5	—	3.5	—
1M-2G	3.8	3.8	3.8	4.4	0.75	1.4	0.75	—	1	1.8	1	—
5M-2G	3.6	3.6	3.6	3.4	—	1	—	—	—	1	—	—
2G-2M	4.5	4.5	4.5	4.9	—	—	—	—	—	—	—	—
7′eqG-1M	—	3	—	—	—	4.6	—	—		3.9	—	—
7′eqG-5M	—	2.6	—	—	—	12	—	—		11	—	—
7′axG-5M	—	2.8	—	—	—	4	—	—		2.8	—	—
7′axG-1M	—	3.9	—	—	—	—	—	—		—	—	—

Comparison between the observed NOEs and those estimated from the calculations according to a full matrix relaxation approach.

Table 3. Chemical shifts (ppm) and relevant coupling constants (Hz) for compounds **1**–**4** at pH 7.0, (D_2O, 500 MHz, 300 K)

Compound **1** ppm (*J*, Hz)		Compound **2** ppm (*J*, Hz)		Compound **3** ppm (*J*, Hz)		Compound **4** ppm (*J*, Hz)	
H1Man	4.29 (1.8, 7.25)	H1Man	5.12 (1.5)	H1Man	4.31(3, 11)	H1Man	5.15 (3.5)
H2Man	3.98 (2.9)	H2Man	4.08 (2.9)	H2Man	3.93 (2.8)	H2Man	4.07 (2.8)
H3Man	3.90 (2.5, 9.1)	H3Man	3.87 (9.1)	H3Man	3.92 (8.8)	H3Man	3.88 (8.8)
H4Man	3.71 (8.8)	H4Man	3.70 (8.8)	H4Man	3.75 (8.9)	H4Man	3.74 (8.9)
H5Man	3.70 (3.0, 4.5)	H5Man	3.76 (3.0, 4.5)	H5Man	3.81 (2.3, 5.5)	H5Man	3.83 (2.3, 5.5)
H6aMan	3.81 (−12.7)	H6aMan	3.88 (−12.7)	H6aMan	3.82 (−12.5)	H6aMan	3.92 (−12.5)
H6bMan	3.91 (−12.5)	H6bMan	3.93	H6bMan	3.86	H6bMan	3.86
O–CH_2	4.17	H7′ax	1.52 (3.8, 9.5, −14.1)			O–CH_2	4.09
HR	1.99 (Table 4)	H7′eq	2.03 (2.5, 2.0)	HR	2.36 (Table 4)	H1′Gal	4.6 (9.0)
HS	2.22 (Table 4)	H2′Gal	3.59 (9.5)	HS	2,12 (Table 4)	H2′Gal	3.68 (3, 9.0)
H1′Gal	3.42 (9.1)	H3′Gal	3.52 (3.0)	H1′Gal	3.31 (9.0)	H3′Gal	3.5 (3.1)
H2′Gal	3.66 (9.5)	H4′Gal	4.09 (1.0)	H2′Gal	3.83 (9.0)	H4′Gal	4.1 (2.6)
H3′Gal	3.49 (3.0)	H5′Gal	1.86 (6.5, 6.9)	H3′Gal	3.71 (3.1)	H5′Gal	3.72
H4′Gal	4.17 (1.0)	H6′aGal	3.64 (−12.1)	H4′Gal	4.22 (2.6)	H6′aGal	3.65
H5′Gal	3.68 (6.5, 6.9)	H6′bGal	3.72	H5′Gal	3.46	H6′bGal	3.64
H6′aGal	3.78 (−12.1)			H6′aGal	3.85		
H6′bGal	3.81			H6′bGal	3.92		

dominant than **B**. No clear evidence of the presence of *anti*-type conformers could be extracted, although it should be small. The agreement between the theoretical NOEs and *J*s obtained from trajectories and the observed experimental data is more than satisfactory. The final conformational distributions of **A**–**E** were 40:45:10:2:3 for **1** and 15:70:10:3:2 for **3**. Thus the aza-*C*-glycoside **3** shows a much higher proportion of *exo*-anomeric conformers at both glycosidic linkages compared with the *C*-glycoside **1**. The carbaglycoside **2** also shows a marked preference for the double *exo*-anomeric conformer **B** (ca. 90%), with minor contributions of non-*exo* conformers at both glycosidic linkages (10%), and a very minor proportion of the *anti*-Φ_{Gal} geometry (conformer **D**). In the case of **4**, the strength of the H1Man–H1Gal and the weakness of the exclusive NOE cross peaks for conformers **A**, **C**–**E** indicate that more than 95% of the population in solution corresponds to conformer **B**. Thus, no major conformational differences are observed between **1** and **4** and their unsubstituted *O*-3 derivatives, **1b** and **4b**.[9] This result is not surprising given the remote position of this modification relative to the glycosidic linkage.

3. Conclusions

Therefore, after combination of molecular mechanics and dynamics calculations and NMR experiments, it may be concluded that the nature of the atoms in the pseudoacetal residue has a pronounced effect on the conformer distribution about the intersaccharide tor-

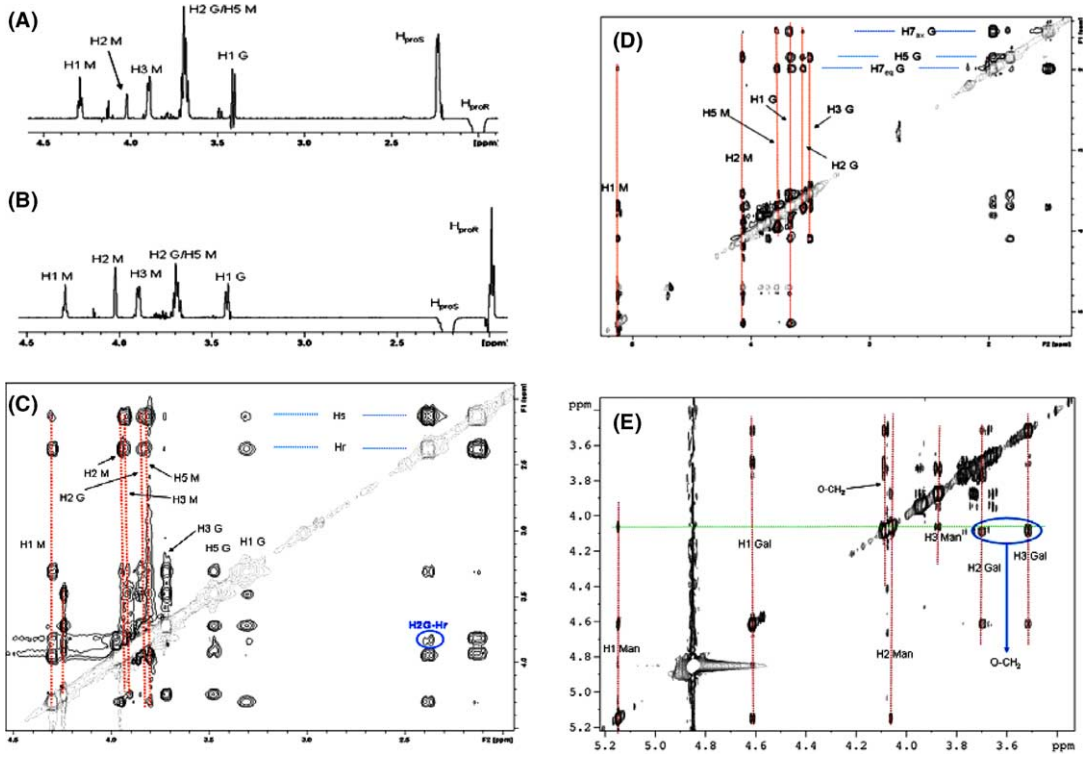

Figure 5. ^{1}H NMR 1D- and 2D-NOESY and T-ROESY data for **1**–**4** at 500 MHz and 300 K in D_2O. Key cross peaks are indicated. (A) Trace of the 2D-T-ROESY spectrum obtained after inversion of HproR of **1**; (B) trace of the 2D-T-ROESY spectrum obtained after inversion of HproS of **1**; (C) 2D-T-ROESY spectrum of **3**; (D) 2D-T-ROESY spectrum of **2**; (E) 2D-T-ROESY spectrum of **4**.

Table 4. Expected *J* values (Hz) for the basic conformations around Φ and Ψ angles for **1** and **3**, deduced by applying the generalized Karplus[20] equation proposed by Altona to the geometries provided by MM3* molecular mechanics calculations

Proton pair	Conformer (*J*, Hz)			Experimental (*J*, Hz)
	exo-Φ	*anti*-Φ	non-*exo*-Φ	
Compound **1**				
GalH-1′/HproS	1.0–1.4	3–6	11.2–11.5	**3.1**
GalH-1′/HproR	10.8–11.3	1.5–3.5	3.2–4.0	**7.7**
ManH-1/HproS	1–2.8	No minimum	11.0–11.6	**7.3**
ManH-1/HproR	10.5–11.6	No minimum	3–4	**7.6**
Compound **3**				
GalH-1′/HproS	11	2.5–4.5	3.2–4.0	**9.4**
GalH-1′/HproR	2–3	2.5–4.5	11.2–11.5	**3.0**
ManH-1/HproS	10.5–11.6	No minimum	4	**10.6**
ManH-1/HproR	1–2.8	No minimum	9–11	**3.0**

sions, relative to the parent *O*-glycoside. *C*-Glycoside **1** and aza-*C*-glycoside **3** present a major conformational averaging around Φ_{Gal} and Φ_{Man} glycosidic linkages with participation of probably five conformers in the conformational equilibrium with fairly small energy barriers among them, in marked contrast with that of the *O*-glycoside **4**, the corresponding *O*-glycosidic analogue.[21]

The high preference for the *exo*/*exo* conformation (**B**) in the case of **4** is expected since this represents two '*exo*-anomeric' effects. By extension the lower population of this conformation in the case of **1** and **3** (i.e., zero *exo*-anomeric effects), is also not surprising, although the relatively high predominance of *exo* rotamers about the Gal glyconic torsion (ca. 85% for both **1** and **3**) is noteworthy. The slightly higher preference for the *exo*/*exo* conformation over the *exo*/non-*exo* conformation (**A**) in **3** versus **1** is also interesting. Given that **1** and **3** only differ at the endocyclic position of the Gal moiety (*O* vs *NH*), it is possible that the different conformational ratios are based in polar effects, the magnitude of which could have been attenuated by the aqueous environment. As noted in our earlier study, it is tempting to speculate on the magnitude of the stereoelectronic contribution of the *exo*-anomeric effect for the Man

α-glyconic bond, by evaluating differences in Gal-*exo*/Man-*exo* and Gal-*exo*/Man-non-*exo* populations for *O*- and *C*-glycoside pairs such as **1** and **4**, and **3** and **4**. Thus, our earlier investigation with **1b** and **4b** suggested a minimum value of 2.1 kcal, which is essentially mirrored in the data for **1** and **4**. Application of this analysis to aza-*C*-glycoside **3** (70:15) and *O*-glycoside **4** (99:1) leads in a value of ca. 1 kcal/mol.

The conformational behaviour of the carbaglycoside **2**, is intermediate between that of **1** and **4**. This may be related to the presence of one '*exo*-anomeric' effect for **2** compared to zero and two contributions in **1** and **4**, respectively.[22] Thus, as might be expected on the basis of the *exo*-anomeric effect for the Man residue, **2** shows a much higher preference for *exo* conformations about the Man glyconic torsion compared with **1** (89 vs 58%). Interestingly, the total *exo* population around the Gal glyconic torsion in **2**, is also increased in **2** relative to **1** (94% in **2** vs 85% in **1**). The difference in geometrical features at the glycosidic linkage of **2** versus **1** (and **3**) is probably at the origin of its conformational behaviour. Indeed, the difference of C–C (ca. 1.54 Å) versus C–O (ca. 1.41 Å) distances, together with the variation of bond angles (C–O–C vs C–C–C values for bond angles) brings the six-membered rings closer in **2**, compared to **1** and **3**, favoring the less sterically congested conformer, **B**.

Finally, the consequence of the relatively low energy differences between the different conformational regions of **1**–**3**, is that it would be possible for selectins or other lectins to bind conformations other than the ground state of the free ligand, without major energy conflicts. This point will be the subject of a subsequent investigation.

4. Experimental

4.1. Materials

The synthesis of these compounds has been described elsewhere.[23]

4.2. Molecular mechanics and dynamics calculations

Potential energy surfaces and population maps were calculated using the MM3* force field, as implemented in MACROMODEL 7.1.[24] The torsion angle Φ_{Man} is defined as H1Man–C1Man–X–C1Gal and Φ_{Gal} as H1Gal–C1Gal–X–C1Man, where X is the atom in the glycosidic bridge. In a first step, a rigid Φ/Ψ map was calculated by using a grid step of 18° at each torsion coordinate. The corresponding 400 conformers were optimized by fixing Φ/Ψ at each corresponding value to generate the relaxed energy map. The probability distribution was calculated from the energy values according to a Boltzmann function at 300 K. In all the molecular mechanics and dynamics calculations, the GB/SA solvation model for water was used.

The molecular dynamics simulations were also performed using the MM3* force field within MACROMODEL 7.1. For molecular dynamics simulations, several geometries, corresponding to the different low energy minima were used as input. A temperature of simulation of 300 K was employed with a time step of 1.5 fs and an equilibration time of 100 ps. The total simulation times for each compound was 8 ns for **1** and **3** (four starting conformers) and 6 ns for **2** (three starting conformers).

4.3. NMR spectroscopy

^{1}H-NMR (500 MHz) spectra were recorded at 30 °C in D_2O, on Varian Unity and Bruker DRX 500 spectrometer. Concentrations of ca. 5 mM of **1**–**4** were used. Chemical shifts are reported in ppm, using external TMS (0 ppm) as reference. The 2D-TOCSY experiment (70 ms mixing time) was performed using a data matrix of $256 \times 2K$ to digitize a spectral width of 3000 Hz. Four scans were used per increment with a relaxation delay of 2 s. 2D-NOESY (300, 400 and 500 ms) and 2D-T-ROESY experiments (300 and 400 ms) used the standard sequences. 1D-Selective NOE spectra were acquired using the double echo sequence proposed by Shaka and co-workers[25] at five different mixing times 200, 400, 600, 800 and 1000 ms were used. NOESY back calculations were performed as described. All the theoretical NOEs calculations were automatically performed by a home-made programme, which is available from the authors upon request.[26,27]

Acknowledgements

The group in Madrid sincerely thank the Ministry of Science of Technology of Spain for financial support (Grants BQU2000-1501-C02 and BQU2003-03550-C03). M.C.F.A. is indebted to the Ministry of Education and Culture of Spain for a Ph.D. fellowship. Funding from the EU (HPRN-CT20002-00173, Glycidic scaffolds) is also acknowledged. The research at Hunter College was supported by Grant GM 57865 from the National Institutes of Health (NIH), and a Research Centers for Minority Institutions (RCMI) award (RR-03037), from the National Center for Research Resources of the NIH.

References

1. (a) *Glycosciences: Status and Perspectives*; Gabius, H.-J., Gabius, S., Eds.; Chapman and Hall: London, Weinheim, 1997; (b) Rüdiger, H.; Siebert, H.-C.; Solís, D.; Jiménez-Barbero, J.; Romero, A.; von der Lieth, C.-W.; Diaz-Mauriño, T.; Gabius, H.-J. *Curr. Med. Chem.* **2000**, *7*, 389–416; (c) Gabius, H.-J.; André, S.; Kaltner, H.; Siebert, H.-C. *Biochim. Biophys. Acta* **2002**, *1572*, 165–177.
2. (a) Witczak, Z. J. *Curr. Med. Chem.* **1999**, *6*, 165; (b) Driguez, H. *Top. Curr. Chem.* **1997**, *187*, 85; (c) Yuasa, H.; Hashimoto, H. Oae. S., Ed.; In *Reviews on Heteroatom Chemistry*; Tokio, 1999; Vol. 19, p 35; (d) Yamazaki, N.; Kojima, S.; Bovin, N. V.; André, S.; Gabius, S.; Gabius, H.-J. *Adv. Drug Deliv. Rev.* **2000**, *43*, 225–244; (e) Davis, B. G.; Robinson, M. A. *Curr. Opin. Drug Discov. Dev.* **2002**, *5*, 279–288.

3. For instance, see: (a) Weatherman, R. V.; Kiessling, L. L. *J. Org. Chem.* **1996**, *61*, 534; (b) Weatherman, R. V.; Mortell, K. H.; Chervenak, M.; Kiessling, L. L.; Toone, E. J. *Biochemistry* **1996**, *35*, 3619; (c) Mikkelsen, L. M.; Hernáiz, M. J.; Martín-Pastor, M.; Skrydstrup, T.; Jiménez-Barbero, J. *J. Am. Chem. Soc.* **2002**, *124*, 14940–14951.
4. (a) Searle, M. S.; Williams, D. H. *J. Am. Chem. Soc.* **1992**, *114*, 10690–10697; (b) Gabius, H.-J. *Pharm. Res.* **1998**, *15*, 23–30; (c) Dam, T. K.; Brewer, C. F. *Chem. Rev.* **2002**, *102*, 387–429.
5. (a) Levy, W.; Chang, D. *Chemistry of C-Glycosides*; Elsevier: Cambridge, 1995; (b) Jiménez-Barbero, J.; Espinosa, J. F.; Asensio, J. L.; Cañada, F. J.; Poveda, A. *Adv. Carbohydr. Chem. Biochem.* **2001**, *56*, 235–284.
6. (a) Lemieux, R. U.; Koto, S.; Voisin, D. *Am. Chem. Soc. Symp. Ser.* **1979**, *87*, 17–29; (b) Kirby, A. J. *The Anomeric Effect and Related Stereoelectronic Effects at Oxygen*; Springer: Heidelberg, Germany, 1983; (c) Tvaroska, I.; Bleha, T. *Adv. Carbohydr. Chem. Biochem.* **1989**, *47*, 45–103; (d) Thatcher, G. R. J. *The Anomeric Effect and Associated Stereoelectronic Effects*; American Chemical Society: Washington, DC, 1993.
7. (a) Kaltner, H.; Stiersdorfer, B. *Acta Anat.* **1998**, *161*, 162–179; (b) Rüdiger, H.; Gabius, H.-J. *Glycoconj. J.* **2001**, *18*, 589–613.
8. Hiruma, K.; Kajimoto, T.; Weitz-Schmidt, G.; Ollman, I.; Wong, C. H. *J. Am. Chem. Soc.* **1996**, *118*, 9265–9270.
9. Asensio, J. L.; Cañada, F. J.; Khan, N.; Mootoo, D. A.; Jiménez-Barbero, J. *Chem. Eur. J.* **2000**, *6*, 1035–1041.
10. (a) Gabius, H.-J.; Darro, F.; Remmelink, M.; André, S.; Kopitz, J.; Danguy, A.; Gabius, S.; Salmon, I.; Kiss, R. *Cancer Invest.* **2001**, *19*, 114–126; (b) Gabius, H.-J. *Biochimie* **2001**, *83*, 659–666.
11. See, for instance: Asensio, J. L.; Espinosa, J. F.; Dietrich, H.; Cañada, F. J.; Schmidt, R. R.; Martin-Lomas, M.; André, S.; Gabius, H.-J.; Jiménez-Barbero, J. *J. Am. Chem. Soc.* **1999**, *121*, 8995–9000.
12. Allinger, N. L.; Yuh, Y. H.; Lii, J. H. *J. Am. Chem. Soc.* **1989**, *111*, 8551–8559.
13. Pearlman, D. A.; Case, D. A.; Caldwell, J. W.; Ross, W. S.; Cheatham, T. E.; DeBolt, S.; Ferguson, D.; Siebal, G.; Kollmann, P. A. *Comput. Phys. Commun.* **1995**, *91*, 1–41.
14. For instance, see: (a) Poveda, A.; Asensio, J. L.; Polat, T.; Bazin, H.; Linhardt, R. J.; Jiménez-Barbero, J. *Eur. J. Org. Chem.* **2000**, 1805–1813; (b) Montero, E.; García-Herrero, A.; Asensio, J. L.; Hirai, K.; Ogawa, S.; Santoyo-González, F.; Cañada, F. J.; Jiménez-Barbero, J. *Eur. J. Org. Chem.* **2000**, *22*, 1945, and references cited therein.
15. Asensio, J. L.; Jiménez-Barbero, J. *Biopolymers* **1995**, *35*, 55–71.
16. Neuhaus, D.; Williamson, M. P. *The Nuclear Overhauser Effect in Structural and Conformational Analysis*; VCH: New York, 1989.
17. For a discussion on the application of molecular mechanics force fields to sugar molecules, see: Perez, S.; Imberty, A.; Engelsen, S.; Gruza, J.; Mazeau, K.; Jimenez-Barbero, J.; Poveda, A.; Espinosa, J. F.; van Eyck, B. P.; Johnson, G. *Carbohydr. Res.* **1998**, *314*, 141–155.
18. For instance, see French, A. D.; Brady, J. W. In *Computer Modelling of Carbohydrate Molecules*. American Chemical Society Symposium Series; 1990.
19. Bock, K.; Duus, J. O. *J. Carbohydr. Chem.* **1994**, *13*, 513–543.
20. Karplus, M. *J. Chem. Phys.* **1959**, *30*, 11.
21. Carpintero, M.; Bastida, A.; Garcia-Junceda, E.; Jimenez-Barbero, J.; Fernandez-Mayoralas, A. *Eur. J. Org. Chem.* **2001**, 4127–4135.
22. Asensio, J. L.; Cañada, F. J.; Jiménez-Barbero, J. *Eur. J. Biochem.* **1995**, *233*, 618–630.
23. (a) Cheng, X.; Kumaran, G.; Mootoo, D. R. *Chem. Commun.* **2001**, 811–812; (b) Cheng, X.; Khan, N.; Kumaran, G.; Mootoo, D. R. *Org. Lett.* **2001**, *3*, 1323–1326.
24. Mohamadi, F.; Richards, N. G. J.; Guida, W. C.; Liskamp, R.; Caufield, C.; Chang, G.; Hendrickson, T.; Still, W. C. *J. Comput. Chem.* **1990**, *11*, 440–467.
25. Stott, K.; Stonehouse, J.; Keeler, J.; Hwang, T.-L.; Shaka, A. J. *J. Am. Chem. Soc.* **1995**, *117*, 4199.
26. Espinosa, J. F.; Cañada, F. J.; Asensio, J. L.; Martín-Pastor, M.; Dietrich, H.; Martín-Lomas, M.; Schmidt, R. R.; Jiménez-Barbero, J. *J. Am. Chem. Soc.* **1996**, *118*, 10862–10871.
27. Espinosa, J. F.; Bruix, M.; Jarreton, O.; Skrydstrup, T.; Beau, J.-M.; Jiménez-Barbero, J. *Chem. Eur. J.* **1999**, 442–448.